1.3 μm Quantum Dot-Distributed Feedback Lasers Directly Grown on (001) Si

Yating Wan, Justin C. Norman, Yeyu Tong, M. J. Kennedy, William He, Jenny Selvidge, Chen Shang, Mario Dumont, Aditya Malik, Hon Ki Tsang, Arthur C. Gossard, and John E. Bowers*

Distributed feedback (DFB) lasers represent a central focus for wavelength-division-multiplexing-based transceivers in metropolitan networks. Here, the first 1.3 μm quantum dot (QD) DFB lasers grown on a complementary metal-oxide-semiconductor (CMOS)-compatible (001) Si substrate are reported. Temperature-stable, single-longitudinal-mode operation is achieved with a side-mode suppression ratio of more than 50 dB and a threshold current density of 440 A cm^{-2}. A single-lane rate of 128 Gbit s^{-1} with a net spectral efficiency of 1.67 $bits^{-1}$ Hz^{-1} is demonstrated, with an aggregate total transmission capacity of 640 Gbit s^{-1} using five channels in the O-band. Apart from the QD active region growth, the overall fabrication is essentially identical to the commercial process for quantum well (QW) DFB lasers. This provides a process-compatible path for QD technology into commercial applications previously filled by QW devices. In addition, the capability to grow laser epi across entire CMOS-compatible (001) Si wafers adds extra benefits of reduced cost, improved heat dissipation, and manufacturing scalability. Through direct epitaxial integration of III–Vs and Si, one can envision a revolution of the photonics industry in the same way that CMOS design and processing revolutionize the microelectronics industry. This is discussed from a system perspective for on-chip optical interconnects.

1. Introduction

The explosive growth of data transmission has fueled a rapid development in wavelength division multiplexing (WDM) techniques in which temperature-stable, single-longitudinal-mode light sources with a predefined channel spacing are a prerequisite.[1] Distributed feedback (DFB) lasers represent an ideal candidate to fulfill these criteria, owing to their single longitudinal mode output, lithographically defined cavity lengths, and adjustable emission wavelengths by changing the grating period. For on-chip interconnect applications, the required large number of optical channels may only be met economically with a monolithic integration approach. While commercially available DFB lasers are predominantly obtained through photonic integration on InP substrates, the yield improvement and manufacturing defect reduction of III–V processing lag far behind the learning curve of Si electrical integrated circuits.[2] A key distinction between the commercial Si and III–V processes is the yield and scaling capability. Si is significantly better, owing to a larger and cheaper wafer, more precise wafer leveling and more advanced lithography tools available after a half-century's development in microelectronics.[3] Regarding this, native III–V devices have been integrated with Si photonic chips through co-packaging and heterogenous integration.[4–7] Since the demonstration of the first prototype of a heterogenously integrated DFB laser on Si,[7] it has only taken ≈10 years to commercialize a 100 Gb s^{-1} integrated Si photonic four-channel course wavelength division multiplexed transmitter, and the industry expects to ramp up to 400 Gb s^{-1} in the next 2 years and then to double or quadruple that rate in just 2 more years.[8]

Meanwhile, monolithic integration of III–V lasers on Si by epitaxial growth offers an elegant and lower cost path to integrate laser sources in a Si photonics platform.[9–14] This field was advanced by transitioning from a quantum well (QW) to quantum dot (QD) active region, which delivers equal or better performance than their predecessors, including low transparency current density,[15–19] high temperature stability,[20–22] low relative

Dr. Y. Wan, Prof. A. C. Gossard, Prof. J. E. Bowers
Institute for Energy Efficiency
University of California Santa Barbara
Santa Barbara, CA 93106, USA
E-mail: yatingwan@ucsb.edu

Dr. J. C. Norman, J. Selvidge, C. Shang, Prof. A. C. Gossard, Prof. J. E. Bowers
Materials Department
University of California Santa Barbara
Santa Barbara, CA 93106, USA

Y. Tong, M. J. Kennedy, W. He, M. Dumont, Dr. A. Malik, Prof. A. C. Gossard, Prof. J. E. Bowers
Department of Electrical and Computer Engineering
University of California Santa Barbara
Santa Barbara, CA 93106, USA

Y. Tong, Prof. H. K. Tsang
Department of Electronic Engineering
The Chinese University of Hong Kong
Shatin, Hong Kong 999077, P. R. China

The ORCID identification number(s) for the author(s) of this article can be found under https://doi.org/10.1002/lpor.202000037

DOI: 10.1002/lpor.202000037

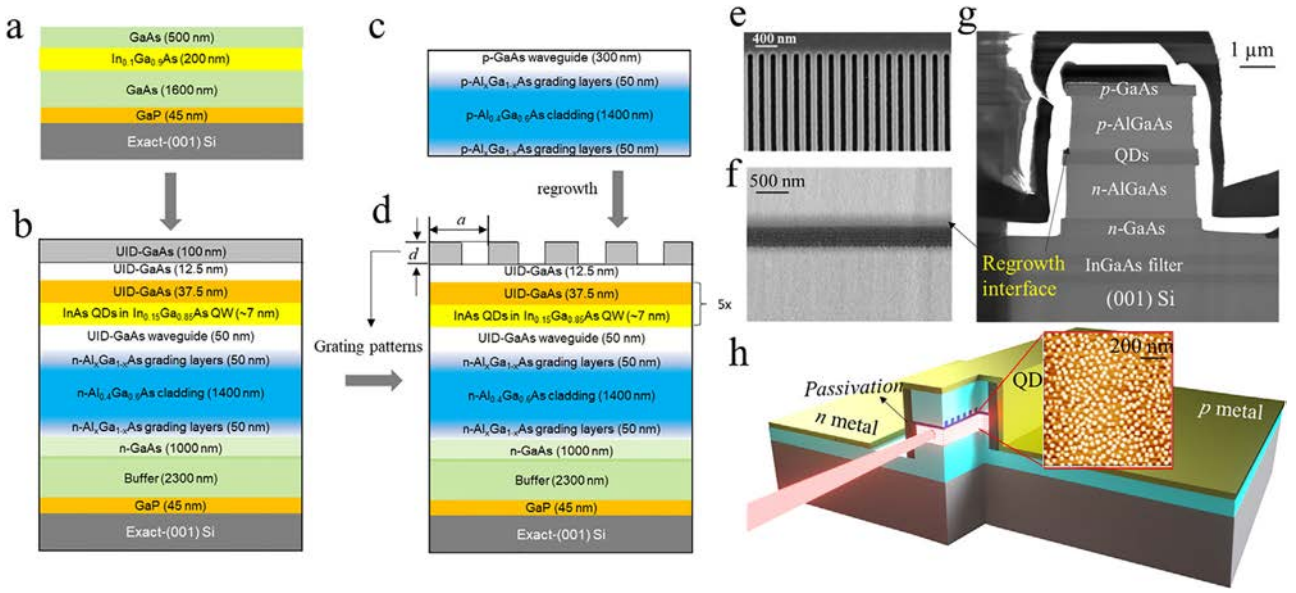

Figure 1. a–d) Schematic image showing the two-step MBE growth. e) Top-view SEM image of the gratings before regrowth. f) Cross-sectional view of diffraction contrast bright field STEM image ($g = 002$) of the regrowth interface. g) Cross-sectional view of axis (110) bright field STEM image and h) schematic image of the fabricated regrown DFB laser.

intensity noise,[23] nearly zero linewidth enhancement factor,[24] tailorable spectral gain bandwidth,[25] significantly reduced sensitivity to external feedback,[26] and large tolerance to material defects.[27–29] While the emphasis for epitaxial III–V on Si research has thus far focused on Fabry–Pérot (FP)-type lasers, yielding rapid progress in reliability with extrapolated lifetimes of more than 100 years at 35 °C, focus has shifted to single frequency lasers.[28] Pioneering work by Wang et al. has demonstrated an array of index-coupled QD DFB lasers epitaxially grown on Si with a record wavelength range covering 100 nm, with a side-mode suppression ratio (SMSR) of up to 50 dB and a threshold current density as low as 550 A cm^{-2} at room temperature (RT).[30] While an aluminum-containing stop-etch layer and a chemically selective etching recipe can be used in InP-based structures to ensure the exact grating etch depth and therefore a precisely controlled grating coupling coefficient (κ), no simple recipes are available in the GaAs/AlGaAs material system. Without a specific etch stop layer in the GaAs/InAs QD material system, accurate control of the etching depth with a high aspect ratio (> 30:1) is challenging. Therefore, for sidewall grating DFBs, the lateral gratings on the laser sidewalls need to be engraved deeply through the active region so that variations of the etching depth are avoided in the vicinity of the optical mode—deviations that would otherwise cause drifting in the effective refractive index and κ along the cavity. This leads to severe nonradiative recombination, reproducibility issues, and increased technical challenges in grating patterning. As a result, no elevated temperature result above RT has been reported and the maximum output power is merely 0.5 mW in the best devices grown on Si.[30] For these devices to be commercially viable, techniques involving reproducible and high-quality regrowth of active layers, similar to the state-of-art QW DFB fabrication, are needed. Furthermore, the reported QD DFB laser structure grown on a Si substrate utilized an off-cut angle of 4° toward the [011] plane to suppress antiphase domains (APDs).[30] Compatibility with the standard Si complementary metal-oxide-semiconductor (CMOS) manufacturing processes provided by on-axis (001) Si wafers is also necessary.

In this article, we report the first 1.3 μm QD DFB lasers grown on a CMOS-compatible (001) Si substrate by molecular beam epitaxy (MBE) regrowth. A process-compatible path is demonstrated to make inroads for the epitaxial QD-based III–V on Si technology into commercial applications previously filled by QW devices on native substrates. Currently, monolithically integrated QW-DFB electro-absorption modulated laser (EML) devices are a well-known route to commercialize externally modulated InP-based devices, and the most successful implementation involves butt-coupled regrowth to spatially modify the bandgap for the modulator and the gain sections.[31] At the end of this manuscript, we describe several integration schemes to integrate QD DFBs and electro-absorption modulators (EAMs) with the aim of process simplicity and high device performance. A concept for a Si terabit transmitter utilizing heteroepitaxial III–V/Si integration is presented. The high-quality MBE regrowth capability provides a process-compatible path to commercialize epitaxial QD-based III–V on Si technology and leads to added flexibility for future device integration.

2. Materials and Device Fabrication

The DFB laser structure was grown on an on-axis (001) GaAs/Si substrate by a two-step MBE process, as illustrated in **Figure 1**a–d. We start with an APD-free GaP/Si (001) on-axis wafer that is commercially available in 300 mm size.[13] A 2300 nm thick GaAs buffer was first grown on top of the GaP/Si substrate in an MBE system by combining a single 200 nm $In_{0.1}Ga_{0.9}As$/GaAs constant composition dislocation filter layer and four periods of

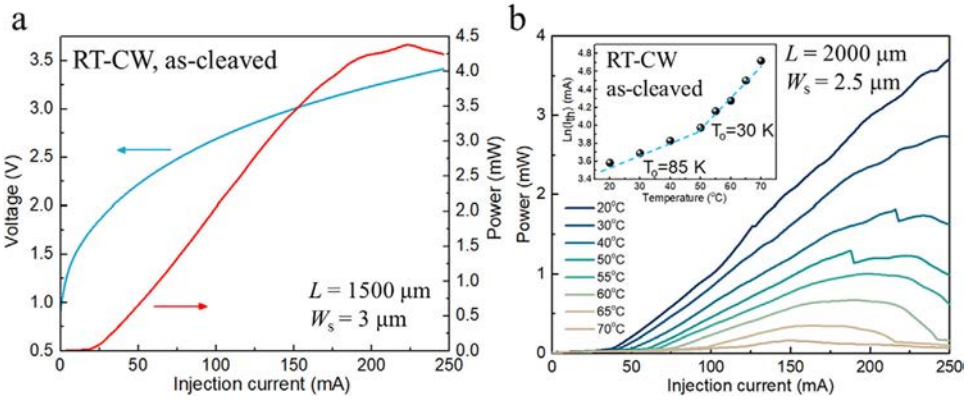

Figure 2. a) Typical *L–I–V* characteristics of an as-cleaved DFB laser with a 3 × 1500 μm^2 cavity. b) High-temperature measurements of a device with a 2.5 × 2000 μm^2 cavity, showing lasing up to 70 °C under CW operation. Inset: natural logarithm of threshold current versus stage temperature. The dashed line represents linear fitting to the experimental data.

thermal cyclic annealing at temperatures between 400 and 725 °C under As_2 overpressure. A low threading dislocation density of 7.3×10^6 cm^{-2} was obtained from the optimized GaAs buffer according to the electron channeling contrast imaging measurement. The n-type GaAs contact layer, AlGaAs lower cladding layers, and the active layers were subsequently grown in which five-stacked InAs QD layers, buried in an InGaAs dot-in-a-well structure, were used to achieve a photoluminescence wavelength close to 1.3 μm, a full-width at half-maximum of 40 nm, and a dot density of $> 5 \times 10^{10}$ cm^{-2}. The 37.5 nm spacer layers above each dot layer contained 10 nm of p-type GaAs to modulation dope the QDs at a level of ≈10 holes per dot. This active region was identical to that described in ref. [16]. A 100 nm uid GaAs layer was grown just above the active layers, and a uniform first-order DFB grating was dry etched into this GaAs layer with an etch depth of 50 nm using an electron beam lithography-patterned SiO_2 hard mask, offering a coupling coefficient κ of roughly 45 cm^{-1}. The grating periods were varied from 195 to 203 nm to obtain emission wavelengths from 1285 to 1340 nm for the WDM laser array. A top-view scanning electron microscopy (SEM) image of the 50:50 surface grating was recorded in Figure 1e. After the grating patterning, the second MBE growth (regrowth) was started with a 2 nm p-GaAs nucleation layer followed by the 1.4 μm upper p-$Al_{0.4}Ga_{0.6}As$ cladding, sandwiched by two 50 nm p-$Al_xGa_{1-x}As$ grading layers, and finished with a 300 nm highly p-doped GaAs contact layer. The pre-regrowth surface treatment was consisted of a solvent clean, O_2 plasma ash, hydrofluoric acid dip, and an in situ atomic H clean for 30 min at 450 °C to remove any native oxide. The high-quality regrowth interface can be visualized through a diffraction contrast bright field scanning transmission electron microscopy (STEM) image ($g = 002$) in Figure 1f.

The as-grown material was then processed into deeply etched waveguide structures in a way similar to that of a standard FP laser. The deeply etched cavity was chosen since it provides strong lateral confinement of photons, carriers, and currents. In QW-based lasers, the carrier in-plane diffusion length reaches several microns and can readily reach the device sidewalls to recombine nonradiatively. The use of QDs in the active region reduces the in-plane diffusion length to ≈0.5 μm. This enhanced carrier localization gives rise to a weaker surface recombination effect. Hence, deep etch through the active layer does not introduce significant penalty on the lasing threshold. However, an unintentional undercut was observed in the AlGaAs cladding likely increasing the optical loss. An i-line (365 nm) step-and-repeat GCA wafer stepper was used to define the ridge waveguides. Inductively coupled plasma with a Cl_2/N_2-based chemistry was used to etch the waveguide with an etching depth of 3.8 μm. After etching, the sidewall was passivated with 12 nm of Al_2O_3 by atomic layer deposition for the initial surface passivation, and subsequently covered with a 500 nm thick SiO_2 layer to fully isolate the optical modes from the Pd/Ti/Pd/Au and Pd/Ge/Pd/Au metal contact stacks. The ridge widths ranged from 1.7 to 3 μm, and the cavity lengths were defined by cleaving after thinning the Si substrate down to 150 μm. No facet coatings were applied and the gratings were defined without quarter lambda cavities. An on-axis cross-sectional bright field diffraction contrast STEM image and the corresponding schematic of the fabricated device are shown in Figure 1g,h, respectively.

3. Measurement and Analysis

Figure 2a shows the light–current–voltage (*L–I–V*) characteristics of a representative device with a cavity length of 1500 μm and a cavity width of 3 μm. The measured 1 V turn-on voltage and 5 Ω differential series resistance from the *I–V* curve indicate good metal contacts and high-quality regrowth interface for efficient current injection. A threshold current of 20 mA was obtained from the *L–I* curve, corresponding to a threshold current density (J_{th}) of 440 A cm^{-2}, or 88 A cm^{-2} per QD layer. Above threshold, the output power followed a kink-free near-linear curve, which is indicative of the mode stability. A maximum output power of 4.4 mW was obtained at an injection current of 220 mA, which was almost an order of magnitude higher than the previously reported Si-based QD DFB laser result.[30] This is important, since a relatively high output power of +4 to +9 dBm is required for DFB lasers to be used in 10G- Ethernet passive optical network (EPON) due to the stringent power budgets.[32] In Figure 2b, *L–I* curves of a device with a 2.5 × 2000 μm^2 cavity show lasing up to 70 °C under continuous wave (CW) operation. On the contrary, only RT operation was reported for the previous Si-based QD DFB laser work.[30] In the inset in Figure 2b, the natural logarithm

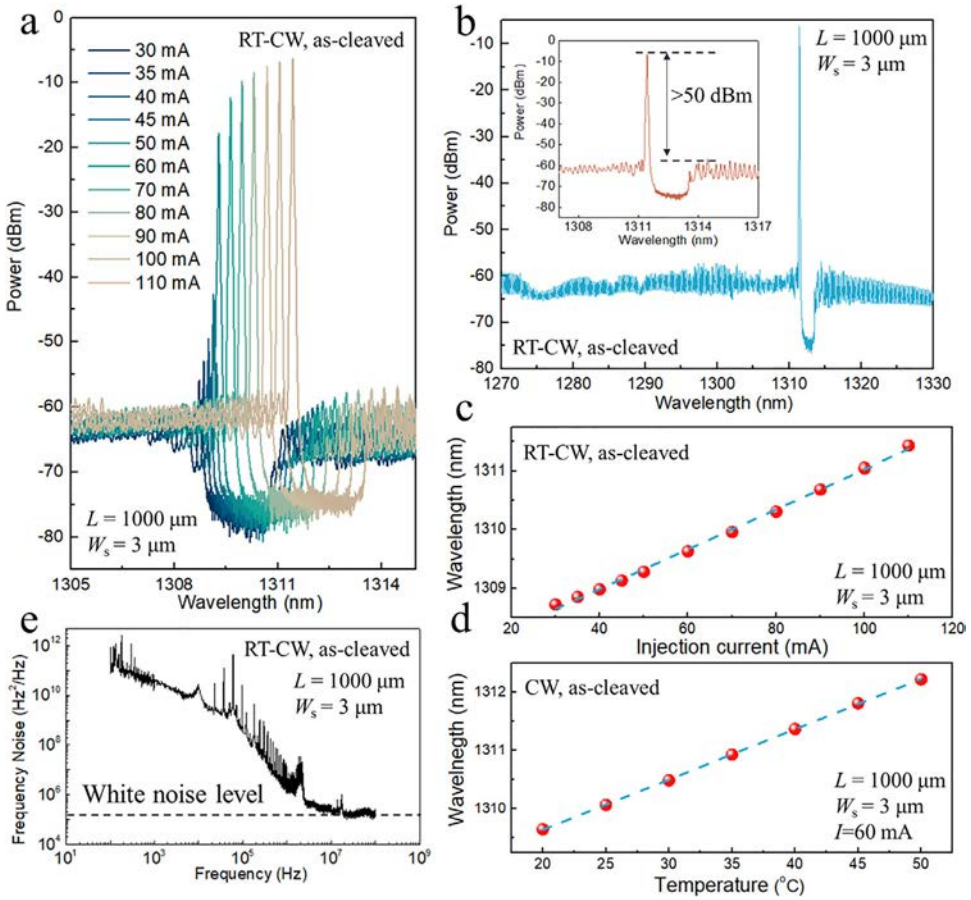

Figure 3. a) Emission spectra with progressively higher injection currents and b) emission spectrum taken at 110 mA for a 3 × 1000 μm^2 device. The corresponding wavelength shift versus c) injection current and d) temperature. e) Frequency noise spectrum of the same device.

of threshold current is plotted as a function of the stage temperature, where the T_0 was extracted to be 85 K between 20 and 50 °C, and 30 K between 50 and 70 °C. Different values of extracted T_0 have been observed in the measured temperature range, which is in agreement with reported results.[33,34] Since the measurements were made under CW operation, the extracted T_0 underestimates the true value due to junction heating, but do make the results representative of performance in real-world applications.

For DFB lasers with uniform gratings, additional reflections are required to destroy the unwanted degeneracy. The reflection from the cleaved facets will have a random relative phase; whereas, optimally it should be in quadrature to shift the net phase from that laser end by the maximum amount. Approximately 40% of the devices were found to lase in a single-longitudinal mode with kink-free *L–I* curves. Representative emission spectra for a 3 × 1000 μm^2 device with progressively higher injection currents are recorded in **Figure 3**a. The laser showed longitudinal and transverse single-mode operation in the ground state across the entire current range, and the peak emission wavelength reached a maximum SMSR of ≈50 dB at an injection current of 110 mA (Figure 3b). In Figure 3c, the extracted central wavelength is plotted as a function of injection current. A current coefficient of wavelength of 0.034 nm mA^{-1} was extracted, which corresponds to a slope of 11.6 nm W^{-1} for the dissipated electric power. In Figure 3d, the temperature dependence of the oscillation wavelength is presented at a fixed injection current of 60 mA. With increasing temperature, the spectral position of the modes slightly shifts at a rate of 0.086 nm °C^{-1} without mode hopping.

One important aspect of QD lasers is the small α factor that contributes to significant reductions in the laser linewidth[35] The state-of-the-art 1550 nm InAs/InP QD DFB lasers can achieve linewidths of less than 50 kHz by applying a very low reflectivity antireflection coating on both facets.[36] For 1300 nm InAs/GaAs QD DFB lasers, the first excited state can be easily populated when increasing the bias.[35] This leads to an asymmetric gain spectrum with increased α factor, and consequently much larger linewidths. However, with highly uniform dot size distributions, the α factor of our InAs/GaAs QD lasers can be as low as 0.13.[24] This leads to a Lorentzian linewidth in these devices of merely 480 kHz (Figure 3e), which is much smaller than the previously reported values in InAs/GaAs QD DFB lasers grown on native substrates, i.e., a linewidth of 5 MHz in ref. [37] and a linewidth of 6 MHz in ref. [38].

The small-signal response of a DFB laser with a cavity size of 3 × 700 μm^2 and a central wavelength of 1.31 μm was analyzed by directly probing the chip using a signal/ground radio frequency (RF) probe. A 20 GHz lightwave component analyzer (HP8703A)

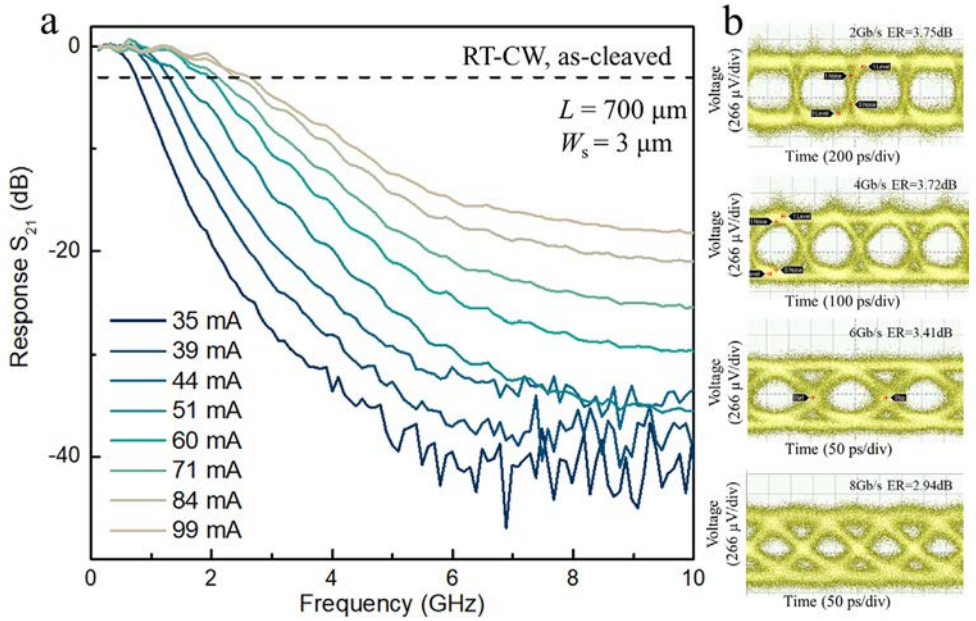

Figure 4. a) Small-signal modulation responses of a regrown DFB laser with a cavity size of 3 × 700 μm^2. b) Eye diagrams of the same DFB laser measured at 2, 4, 6, and 8 Gbit s^{-1} at a bias current of 100 mA.

was used. As shown in **Figure 4**a, the injected currents were varied from 35 to 99 mA, and a 3 dB bandwidth of 2.8 GHz was attained at a bias current of 99 mA. No mode hoping was observed with the application of modulated injection currents. Eye diagrams of the same device were directly captured by a photoreceiver with a trans-impedance amplifier (FINISAR XPRV2022A) and a sampling oscilloscope (Agilent DCA 86100A). For this back to-back (B2B) transmission, the DC bias current was fixed at 100 mA, and a non-return-to-zero pseudo-random bit sequence signal, which was generated by a signal quality analyzer (Anritsu MP1800A) with a peak-to-peak voltage of 2 V, was used to drive the laser. Since previous studies have shown that QD lasers exhibit over 1 00 000 (or 50 dB) increase in the critical feedback level compared to the QW counterparts such that coherence collapse does not occur even with 90% of the light reflected back to the laser,[24] no isolator was used during the on-off keying measurement. The captured eye diagrams at 2, 4, 6, and 8 Gbit s^{-1} are presented in Figure 4b, with an extinction ratio of 3.75, 3.72, 3.41, and 2.94 dB, respectively. Clear eye openings can only be observed up to 8 Gb s^{-1}, limited by the 3 dB bandwidth of the laser. Compared to InP-based 25 Gb s^{-1} high speed DFB lasers, which are currently used for commercial optical fiber communications, the 8 Gb s^{-1} data rate for the presented QD laser has limited its application in the same scenario, but the proof of concept has been demonstrated for native substrate InAs QD laser with properly optimized designs.[39] Currently, the 10 Gb s^{-1} × 10 lane architectures deployed in data centers have also spawned intense interest in exploring inexpensive low-bandwidth lasers. By reducing the cavity length with an increased number of active QD layers and high-reflectivity facet coatings, and minimizing the electrode pad capacitance with a several micron-thick benzocyclobutene passivation layer, the 3 dB bandwidth of the low-cost QD DFB lasers directly grown on Si can be improved to some extent.[40,41] Therefore, these lasers should be usable in 10 Gb s^{-1} EPONs, which represent the leading technology for 5G mobile networks.

However, a high-modulation bandwidth has been recognized as difficult to attain for QD lasers.[40,42] Due to the inherently finite intra-band relaxation time and gain saturation effect,[43] the best reported modulation bandwidth of 1.3 μm QD DFB lasers grown on native substrates is limited to around 10 GHz.[44] Meanwhile, externally modulated QD DFB lasers as optical sources are attractive since these devices do not require isolators to avoid feedback effects. A low wavelength chirp is also expected compared with the directly modulated lasers. From various bars distributed across a wafer, over 50 nm wavelength coverage could be achieved by a five-wavelength QD DFB laser array in the 1.3 μm communication band. In **Figure 5**a, the spectra of the five devices measured at RT are superimposed, with SMSRs from 45 to 50 dB and emission wavelengths from 1285 to 1338 nm. This wavelength range was limited not by the QDs but rather by the range of grating periods fabricated. The inhomogenous broadening of QD gain materials leads to an advantageously wide useable gain bandwidth that can be engineered in growth. By deploying a chirped design in the QD region, a significantly broadened gain bandwidth of 127 nm can be experimentally attained.[25] Therefore, the emission wavelength can be extended well beyond the current test range controlled by the current grating period variation (Figure 5b). This predicts a huge potential application for on-chip WDM within the O-band, according to the IEEE802.3ba standard.

As a proof-of-concept demonstration, a laser with a center wavelength at 1311 nm of the five channels shown in Figure 5a was utilized as an optical carrier, which was amplified by a praseodymium-doped fiber amplifier to compensate for the fiber coupling loss before being external modulation by a 30 GHz lithium niobate Mach–Zehnder modulator (IXblue MX1300-LN-40). The 128 Gbit s^{-1} electrical PAM-4 signals generated by an

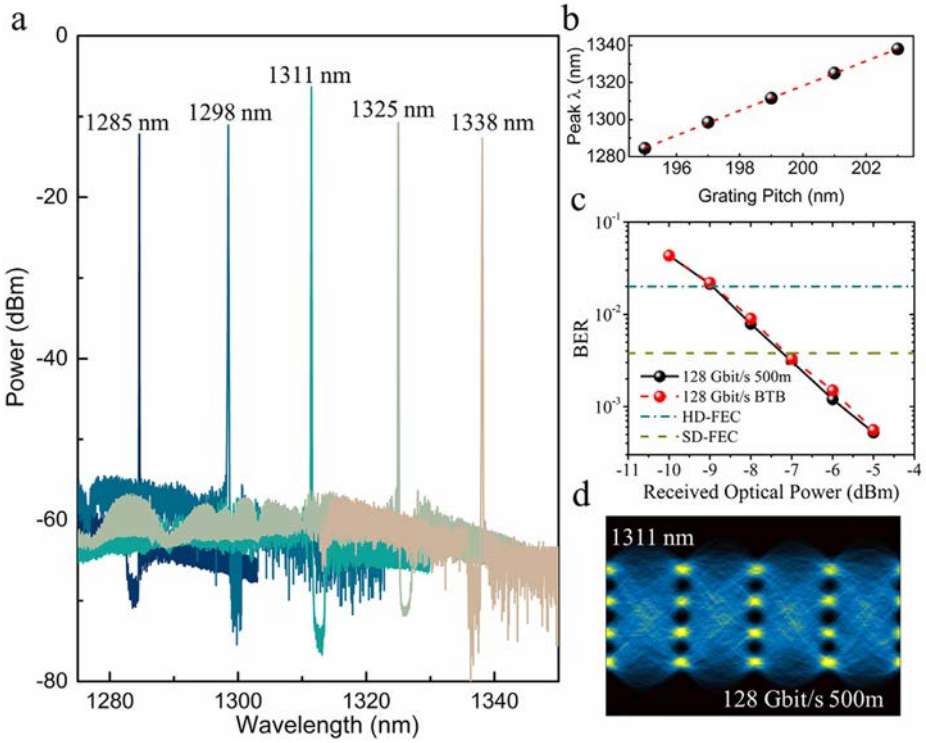

Figure 5. a) Superimposed spectra of the five-wavelength QD DFB laser array measured at RT. The emission wavelength covers 1285 to 1338 nm. b) Correlation between the grating period and the emission wavelength of DFB lasers. c) BER versus received optical power for B2B and after 500 m SSMF transmission using the laser with a center emission at 1311 nm. d) Corresponding eye diagram after 500 m SSMF transmission.

arbitrary waveform generator (Keysight M8196A, with 32 GHz analog bandwidth and 92 GSa s^{-1} sampling rate) are amplified to ≈3.5 V peak-to-peak by a 38 GHz broadband RF amplifier (SHF 806E). The received optical power is controlled by using a variable optical attenuator before the photodetector (Finisar XPRV2022A). Details of the digital signal processing (DSP) for PAM-4 signal transmission and detection can be accessed in ref. [45]. The modulated optical signal is transmitted for back-to-back (B2B) and 500 m standard single-mode fiber (SSMF) characterization, respectively. Finally, the electrical signal is sampled by a 70 GHz real-time oscilloscope (Tektronix DPO77002SX) at 200 GSa s^{-1} and is processed by the receiver DSP for signal demodulation and error counting. A representative bit-error-ratio (BER) versus the received optical power is plotted in Figure 5c. Minimal power penalties were observed between the B2B and 500 m SSMF transmission due to the low fiber dispersion penalty at 1311 nm. The hard-decision forward error correction (HD-FEC) threshold at 3.8×10^{-3} (7% overhead) and the soft-decision forward error correction (SD-FEC) threshold at 2.0×10^{-2} (20% overhead) have been labeled. A single-lane rate of 128 Gbit s^{-1} with a net spectral efficiency of 1.67 $bits^{-1}$ Hz^{-1} considering the overhead of 7% for the HD-FEC is experimentally demonstrated. For the three tested channels from 1285 to 13 111 nm, the BERs are below the SD-FEC at received optical power from −5 to −7 dBm and are below the HD-FEC at received optical power between −5 and −9 dBm. The channels at 1325 and 1338 nm were not tested for external modulation in our experiment due to the optical bandwidth limitation of the available modulator. An aggregate data rate of over 640 Gbit s^{-1} using the five DFB lasers would be feasible in the future by optimizing the wavelengths of the DFB laser arrays.

4. Discussion and Outlook

The main focus of this work is to develop a process-compatible path to make inroads for the epitaxial QD-based III–V on Si technology into commercial applications, similar to that of InP-based photonic integrated circuits (PICs). A proof-of-concept demonstration of an aggregate data rate of over 640 Gbit s^{-1} has been made using five externally modulated QD DFB laser arrays. In pursuing this approach, monolithic integration of DFB lasers and EAMs into a single two-section device needs to be investigated and the integration process should preserve the properties of the two components as well as ensure efficient optical waveguide coupling. Various photonic integration schemes with epitaxial III–V on Si have been devised, including: coupling light generated in the QD section to the Si waveguide in a silicon on insulator substrate, depositing foreign waveguides, and fully III–V-based integration with waveguide layers grown in the epi stack.[17] In the final approach, the entire PIC is self-contained within epitaxially deposited III–V layers on Si, analogous to the case of photonic integration on InP, but with a major distinction being that the III–V layers are grown on a much cheaper, more robust, and larger Si substrate. In **Figure 6**a, we focus on two possible integration schemes with the aim of process simplicity and high-device performance. The final two-section device consists of a QD DFB laser and a modulator. The DFB laser provides a

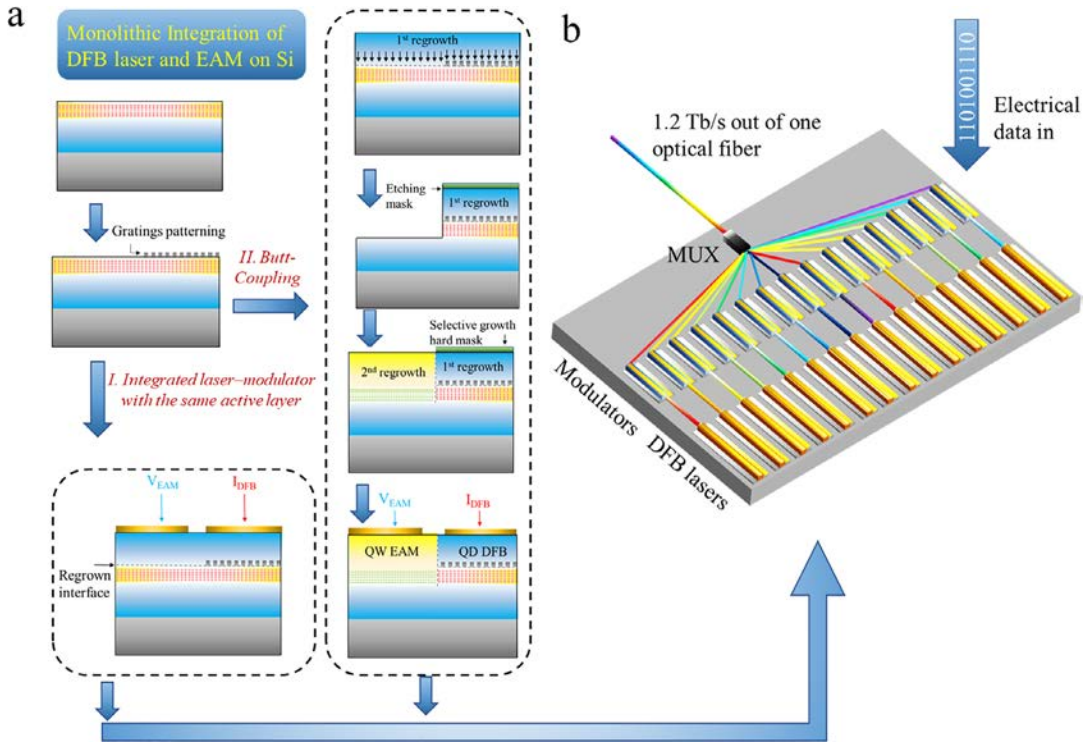

Figure 6. a) Two integration schemes to achieve monolithic integrated QD-based DFB-EML on Si. b) A concept for a Si terabit transmitter utilizing monolithically integrated QD-DFB EML.

constant single-mode emission with low chirp and low sensitivity to temperature variations and optical feedback. The data rate achieved by direct modulation can be exceeded by using EAMs that modulate the output power based on the quantum-confined Stark effect.

Path I represents the simplest method where the DFB lasers and EAMs are integrated with the same active layer comprised of QDs without multiple regrowths. Separately, QD DFB lasers and QD EAMs have been demonstrated on native substrates, where the QD EAMs possess a 3 dB bandwidth of 17 GHz and an extinction ratio of 18 dB.[46] The viability of this common QD-active EML scheme has been investigated based on a spectroscopic study of the optical gain and absorption, which shows that the amount of detuning for optimal wavelength compatibility between lasing and modulation is achievable by virtue of the inherently wide gain spectrum of QDs.[47] Since high-gain, high-saturation amplifiers,[48] and ultra-low dark current photodetectors[49–51] have already been demonstrated sharing the same material with the QD-based lasers, the addition of a modulator could enable a simple, manufacturable method of photonic integration without multiple regrowth. The process simplicity of this common QD-active approach allows device integration on the same chip not only for a laser–modulator system (schematically plotted in Figure 6a) but also for a tandem of integrated PIC links with DFB lasers, modulators, optical amplifiers, and photodetectors. However, this approach does not allow independent optimization of the laser and the modulator, and the wavelength compatibility of different devices can become an important issue in the integration process.

For QW devices, a well-known route to monolithically integrate DFB-EML devices relies upon butt-coupled regrowth to spatially vary the band-gap, and 40 Gbit s^{-1} transmission has been demonstrated using a conventional etching and regrowth process.[52] In Path II, the same technology is synchronously leveraged for the epitaxial QD-based III–V on Si technology. After the regrowth of the DFB laser upper cladding, selective etching will be performed and the modulator layers are subsequently regrown, allowing independent design of the laser and modulator active layers. The parallel efforts in the QW-based regrown DFB-EML devices on native InP substrates provide many insights into managing etching and regrowth steps to achieve efficient optical coupling between the two waveguides, and accurate alignment of the absorption band edge of the EMLs with respect to the DFB lasing wavelengths. The high-performance regrown QD DFB lasers demonstrated here are clearly indicative of the high-quality MBE regrowth capability in GaAs-based materials, but metal-organic chemical vapor deposition-based regrowth is equally applicable. This provides a process-compatible path to commercialize epitaxial QD-based III–V on Si technology, similar to that of InP-based PICs. In Figure 6b, a concept for a Si transmitter utilizing heteroepitaxial integration is presented. The monolithic integrated DFB lasers are externally modulated and then multiplexed together into a single waveguide to form a WDM data stream. An aggregated data rate of over 1 Tb s^{-1} can even be envisioned in the future, though all the tradeoffs such as the cost, the single-lane data rate, the modulator optical bandwidth, the wavelength spacing, and the number of WDM channels must be considered. The integrated transmitter is

expected to be energy-efficient and compatible with the 300 mm diameter wafer size high-volume manufacturing. The prospects for photonic integration via epitaxial growth on Si are bright, but much remains to be done to propel it to the market place. Some key remaining challenges have been outlined in ref. [53]. In addition, it should be noted that by confining all functional devices to III–V layers, Si is reduced to a mere substrate. This raises a whole range of issues with regard to the relationship between a Si-based epi laser and Si photonics. While Si is a larger and cheaper substrate, the reduced yield and reliability due to poorer material quality compared to lattice matched substrate growth and simply the need to grow thick buffer layers (hence higher growth costs) may overcome the advantages of a Si substrate. Solving these problems is the subject of ongoing research. In addition, the limited optical bandwidth of the EAM would be a significant challenge in the possible pathways, in order to enable the ultimate potentials to obtain as high as possible aggregated data rate.

Supporting Information

Supporting Information is available from the Wiley Online Library or from the author.

Acknowledgements

Y.W., J.N., and Y.T. contributed equally to this work. The information, data, or work presented herein was funded in part by the Advanced Research Projects Agency-Energy (ARPA-E), U.S. Department of Energy, under Award Number DE-AR0001042 and DE-AR0001039. The views and opinions of authors expressed herein do not necessarily state or reflect those of the United States Government or any agency thereof. The authors are grateful to Dr. Daehwan, Dr. Di Liang, Dr. Chong Zhang, Dr. Bill Mitchell, Dr. Songtao Liu, and Chao Xiang for helpful discussion and the support from the nanofabrication facilities at the University of California, Santa Barbara.

Conflict of Interest

The authors declare no conflict of interest.

Keywords

heteroepitaxy, quantum dot lasers, Si photonics

Received: February 1, 2020
Revised: April 10, 2020
Published online:

[1] Q. Cheng, M. Bahadori, M. Glick, S. Rumley, K. Bergman, *Optica* **2018**, *5*, 1354.
[2] G. E. Hoefler, Y. Zhou, M. Anagnosti, A. Bhardwaj, P. Abolghasem, A. James, S. Luna, P. Debackere, A. Dentai, T. Vallaitis, P. Liu, M. Missey, S. Corzine, P. Evans, V. Lal, M. Ziari, D. Welch, F. Kish, J. S. Suelzer, P. S. Devgan, N. G. Usechak, *IEEE J. Sel. Top. Quantum Electron.* **2019**, *25*, 1.
[3] G. Roelkens, L. Liu, D. Liang, R. Jones, A. Fang, B. Koch, J. Bowers, *Laser Photonics Rev.* **2010**, *4*, 751.
[4] J. Zhang, B. Haq, J. O'Callaghan, A. Gocalinska, E. Pelucchi, A. J. Trindade, B. Corbett, G. Morthier, G. Roelkens, *Opt. Express* **2018**, *26*, 8821.
[5] S. Uvin, S. Kumari, A. De Groote, S. Verstuyft, G. Lepage, P. Verheyen, J. Van Campenhout, G. Morthier, D. Van Thourhout, G. Roelkens, *Opt. Express* **2018**, *26*, 18302.
[6] H. Duprez, C. Jany, C. Seassal, B. Ben Bakir, *Opt. Express* **2016**, *24*, 20895.
[7] C. Xiang, W. Jin, J. Guo, J. D. Peters, M. Kennedy, J. Selvidge, P. A. Morton, J. E. Bowers, *Optica* **2020**, *7*, 20.
[8] R. Jones, P. Doussiere, J. B. Driscoll, W. Lin, H. Yu, Y. Akulova, T. Komljenovic, J. E. Bowers, *IEEE Nanotechnol. Mag.* **2019**, *13*, 17.
[9] Z. Zhou, B. Yin, J. Michel, *Light: Sci. Appl.* **2015**, *4*, e358.
[10] Y. Hu, D. Liang, K. Mukherjee, Y. Li, C. Zhang, G. Kurczveil, X. Huang, R. G. Beausoleil, *Light: Sci. Appl.* **2019**, *8*, 1.
[11] Z. Wang, A. Abbasi, U. Dave, A. De Groote, S. Kumari, B. Kunert, C. Merckling, M. Pantouvaki, Y. Shi, B. Tian, K. Van Gasse, J. Verbist, R. Wang, W. Xie, J. Zhang, Y. Zhu, J. Bauwelinck, X. Yin, Z. Hens, J. Van Campenhout, B. Kuyken, R. Baets, G. Morthier, D. Van Thourhout, G. Roelkens, *Laser Photonics Rev.* **2017**, *11*, 1700063.
[12] M. Liao, S. Chen, S. Chen, S. Huo, J. Wu, M. Tang, K. Kennedy, W. Li, S. Kumar, M. Martin, T. Baron, C. Jin, I. Ross, A. Seeds, H. Liu, *IEEE J. Sel. Top. Quantum Electron.* **2017**, *23*, 1.
[13] J. C. Norman, D. Jung, Y. Wan, J. E. Bowers, *APL Photonics* **2018**, *3*, 030901.
[14] Z. Mi, J. Yang, P. Bhattacharya, G. Qin, Z. Ma, *Proc. IEEE* **2009**, *97*, 1239.
[15] S. Chen, W. Li, J. Wu, Q. Jiang, M. Tang, S. Shutts, S. N. Elliott, A. Sobiesierski, A. J. Seeds, I. Ross, P. M. Smowton, H. Liu, *Nat. Photonics* **2016**, *10*, 307.
[16] C. Shang, Y. Wan, J. C. Norman, N. Collins, I. MacFarlane, M. Dumont, S. Liu, Q. Li, K. M. Lau, A. C. Gossard, J. E. Bowers, *IEEE J. Sel. Top. Quantum Electron.* **2019**, *25*, 1.
[17] Y. Wan, J. Norman, J. Bowers, *Future Directions in Silicon Photonics*, Semiconductors and Semimetals, Vol. *101*, Academic Press, San Diego, CA **2019**.
[18] T. Zhou, M. Tang, G. Xiang, X. Fang, X. Liu, B. Xiang, S. Hark, M. Martin, M.-L. Touraton, T. Baron, Y. Lu, S. Chen, H. Liu, Z. Zhang, *Optica* **2019**, *6*, 430.
[19] Y. Wan, J. Norman, Q. Li, M. J. Kennedy, D. Liang, C. Zhang, D. Huang, Z. Zhang, A. Y. Liu, A. Torres, D. Jung, A. C. Gossard, E. L. Hu, K. M. Lau, J. E. Bowers, *Optica* **2017**, *4*, 940.
[20] J. Kwoen, B. Jang, K. Watanabe, Y. Arakawa, *Opt. Express* **2019**, *27*, 2681.
[21] N. Kryzhanovskaya, E. Moiseev, Y. Polubavkina, M. Maximov, M. Kulagina, S. Troshkov, Y. Zadiranov, Y. Guseva, A. Lipovskii, M. Tang, M. Liao, J. Wu, S. Chen, H. Liu, A. Zhukov, *Opt. Lett.* **2017**, *42*, 3319.
[22] Y. Wan, Q. Li, A. Y. Liu, A. C. Gossard, J. E. Bowers, E. L. Hu, K. M. Lau, *Appl. Phys. Lett.* **2016**, *109*, 011104.
[23] M. Liao, S. Chen, Z. Z. Liu, Y. Wang, L. Ponnampalam, Z. Zhou, J. Wu, M. Tang, S. Shutts, Z. Z. Liu, P. M. Smowton, S. Yu, A. Seeds, H. Liu, *Photonics Res.* **2018**, *6*, 1062.
[24] J. Duan, H. Huang, B. Dong, D. Jung, J. C. Norman, J. E. Bowers, F. Grillot, *IEEE Photonics Technol. Lett.* **2019**, *31*, 345.
[25] Y. Wan, S. Zhang, J. C. Norman, M. J. Kennedy, W. He, S. Liu, C. Xiang, C. Shang, J.-J. He, A. C. Gossard, J. E. Bowers, *Optica* **2019**, *6*, 1394.
[26] H. Huang, J. Duan, D. Jung, A. Y. Liu, Z. Zhang, J. Norman, J. E. Bowers, F. Grillot, *J. Opt. Soc. Am. B* **2018**, *35*, 2780.
[27] Y. Wan, Q. Li, A. Y. Liu, A. C. Gossard, J. E. Bowers, E. L. Hu, K. M. Lau, *Opt. Lett.* **2016**, *41*, 1664.
[28] D. Jung, Z. Zhang, J. Norman, R. Herrick, M. J. Kennedy, P. Patel, K. Turnlund, C. Jan, Y. Wan, A. C. Gossard, *ACS Photonics* **2018**, *5*, 1094.

[29] Q. Feng, W. Wei, B. Zhang, H. Wang, J. Wang, H. Cong, T. Wang, J. Zhang, *Appl. Sci.* **2019**, *9*, 385.
[30] Y. Wang, S. Chen, Y. Yu, L. Zhou, L. Liu, C. Yang, M. Liao, M. Tang, Z. Liu, J. Wu, W. Li, I. Ross, A. J. Seeds, H. Liu, S. Yu, *Optica* **2018**, *5*, 528.
[31] A. Ramdane, F. Devaux, N. Souli, D. Delprat, A. Ougazzaden, *IEEE J. Sel. Top. Quantum Electron.* **1996**, *2*, 326.
[32] K. Tanaka, A. Agata, Y. Horiuchi, *J. Lightwave Technol.* **2010**, *28*, 651.
[33] J. C. Norman, Z. Zhang, D. Jung, C. Shang, M. Kennedy, M. Dumont, R. W. Herrick, A. C. Gossard, J. E. Bowers, *IEEE J. Quantum Electron.* **2019**, *55*, 1.
[34] L. V. Asryan, R. A. Suris, *Semiconductors* **2004**, *38*, 1.
[35] T. Septon, A. Becker, S. Gosh, G. Shtendel, V. Sichkovskyi, F. Schnabel, A. Sengül, M. Bjelica, B. Witzigmann, J. P. Reithmaier, G. Eisenstein, *Optica* **2019**, *6*, 1071.
[36] T. Septon, S. Gosh, A. Becker, V. Sichkovskyi, F. Schnabel, A. Rippien, J. P. Reithmaier, G. Eisenstein, in *2019 Optical Fiber Communications Conf. and Exhibition*, Optical Society of America, San Diego, CA **2019**, pp. 1–3.
[37] H. Su, L. F. Lester, *J. Phys. D: Appl. Phys.* **2005**, *38*, 2112.
[38] J. Kim, S. L. Chuang, *IEEE J. Quantum Electron.* **2006**, *42*, 942.
[39] M. Ishida, M. Matsuda, Y. Tanaka, K. Takada, M. Ekawa, T. Yamamoto, T. Kageyama, M. Yamaguchi, K. Nishi, M. Sugawara, Y. Arakawa, in *CLEO: Science and Innovations*, Optical Society of America, San Jose, CA **2012**, p. CM1I.2.
[40] C. Hantschmann, P. P. Vasil'Ev, A. Wonfor, S. Chen, M. Liao, A. J. Seeds, H. Liu, R. V. Penty, I. H. White, *J. Lightwave Technol.* **2019**, *37*, 949.
[41] D. Inoue, D. Jung, J. Norman, Y. Wan, N. Nishiyama, S. Arai, A. C. Gossard, J. E. Bowers, *Opt. Express* **2018**, *26*, 7022.
[42] Y. Wan, S. Zhang, J. C. Norman, M. Kennedy, W. He, Y. Tong, C. Shang, J. He, H. K. Tsang, A. C. Gossard, J. E. Bowers, *Laser Photonics Rev.* **2020**, *14*, 1900348.
[43] A. Fiore, A. Markus, *IEEE J. Quantum Electron.* **2007**, *43*, 287.
[44] K. Takada, Y. Tanaka, T. Matsumoto, M. Ekawa, H. Z. Song, Y. Nakata, M. Yamaguchi, K. Nishi, T. Yamamoto, M. Sugawara, Y. Arakawa, *Electron. Lett.* **2011**, *47*, 206.
[45] Y. Tong, Z. Hu, X. Wu, S. Liu, L. Chang, A. Netherton, C.-K. Chan, J. E. Bowers, H. K. Tsang, *IEEE Photonics Technol. Lett.* **2019**, *32*, 125.
[46] D. Bimberg, M. Stubenrauch, G. Stracke, H. Schmeckebier, D. Arsenijevic, in *2012 14th Int. Conf. Transparent Optical Networks (ICTON)*, IEEE, Piscataway, NJ **2012**, pp. 1–4.
[47] S. A. Sobhani, B. J. Stevens, N. Babazadeh, K. Takemasa, K. Nishi, M. Sugawara, R. A. Hogg, D. T. D. Childs, *IEEE Photonics Technol. Lett.* **2019**, *31*, 419.
[48] S. Liu, J. Norman, M. Dumont, D. Jung, A. Torres, A. C. C. Gossard, J. E. E. Bowers, *ACS Photonics* **2019**, *6*, 2523.
[49] Y. Wan, Z. Zhang, R. Chao, J. Norman, D. Jung, C. Shang, Q. Li, M. Kennedy, D. Liang, C. Zhang, J.-W. Shi, A. C. Gossard, K. M. Lau, J. E. Bowers, *Opt. Express* **2017**, *25*, 27715.
[50] J. Huang, Y. Wan, D. Jung, J. Norman, C. Shang, Q. Li, K. M. Lau, A. C. Gossard, J. E. Bowers, B. Chen, *ACS Photonics* **2019**, *6*, 1100.
[51] B. Tossoun, G. Kurczveil, C. Zhang, A. Descos, Z. Huang, A. Beling, J. C. Campbell, D. Liang, R. G. Beausoleil, *Optica* **2019**, *6*, 1277.
[52] Uncooled Operation of 10-/40-Gbit/s 1.55-μm Electroabsorption Modulator Integrated with Distributed Feedback Laser https://www.ntt-review.jp/archive/ntttechnical.php?contents=ntr201008le2.html (accessed: May 2020).
[53] A. Y. Liu, J. Bowers, *IEEE J. Sel. Top. Quantum Electron.* **2018**, *24*, 1.